Available online at www.sciencedirect.com

jmr&t Journal of Materials Research and Technology

journal homepage: www.elsevier.com/locate/jmrt

Original Article

Effect of cryogenic treatment on tribological behavior of Ti6Al4V alloy fabricated by selective laser melting

Xina Huang [a,b,*], *Shoubin Ding* [a], *Wen Yue* [a,b,**]

[a] School of Engineering and Technology, China University of Geosciences (Beijing), Beijing, 100083, China
[b] Zhengzhou Institute, China University of Geosciences (Beijing), Zhengzhou, 451283, China

ARTICLE INFO

Article history:
Received 19 December 2020
Accepted 6 April 2021
Available online 11 April 2021

Keywords:
Selective laser melting (SLM)
Ti6Al4V
Cryogenic treatment (CT)
Tribological behavior

ABSTRACT

Ti6Al4V fabricated by selective laser melting (SLM) is commonly used as an artificial hip joint. However, the inferior tribological properties fall far short of the requirements for biomedical engineering and is harmful to the patients. In this study, cryogenic treatment (CT) was proposed to solve this problem. CT at −196 °C with a soaking time of both 2 h and 72 h were conducted, and their tribological properties were investigated by microstructure observation, Vickers hardness, and wear tests. The results showed that the microstructure of the as-fabricated and cryogenic treated (CTed) for 2 h are mainly composed of acicular martensite (α′ phase). However, the microstructure is transformed into alpha and beta phases after CT for 72 h. Vickers hardness of the specimens as-fabricated, CTed for 2 h and 72 h are 390.79 HV, 388.03 HV, and 371.34 HV, respectively. CT induces a significant improvement in tribological properties, which is correlated with the microstructure evolution. A similar wear mechanism can be observed for the specimens as-fabricated and CTed for 2 h, which is the co-action of severe abrasive wear, adhesive wear, and fatigue wear. While the specimen CTed for 72 h is slight abrasive wear mechanism.

1. Introduction

At present, the osteoarthritis and femoral head necrosis are very common diseases, which severely affect people's lives [1–3]. Total hip arthroplasty (THA) offers an excellent solution against continuous necrosis of the bone [4–6]. However, the artificial hip joint contacted with the hard natural bones of the human body is susceptible to wear, resulting in the late loosening of the replacement joint, joint inflammation and pain, and even joint replacement failure [4,7]. Besides, the abrasive debris may go to blood, tissue, lymph nodes, and bone marrow, which also are harmful to the human body [8].

Ti6Al4V is one of the most common biomaterials due to its excellent biocompatibility, low Young's modulus, high specific strength, and corrosion resistance [9,10]. However, its large-scale application is restricted by two factors. Firstly, Ti6Al4V is difficult to process and the processing cost is high.

* Corresponding author.
** Corresponding author.
E-mail addresses: huangxina@126.com (X. Huang), cugbyw@163.com (W. Yue).
https://doi.org/10.1016/j.jmrt.2021.04.012

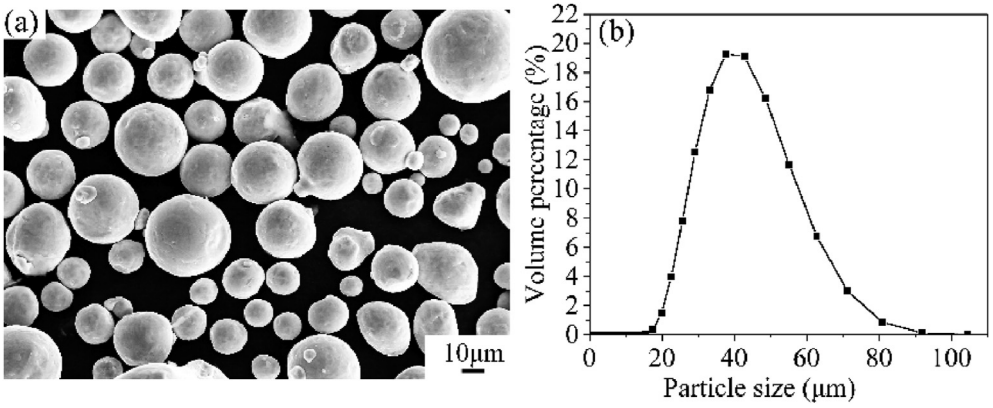

Fig. 1 – Ti6Al4V powder: (a) SEM morphology; (b) particle size distribution.

The emergence of additive manufacturing (AM) technologies provides the possibility to solve this problem. Among these technologies, selective laser melting (SLM) is one of the most widely used, which can directly produce three-dimensional (3D) parts by a laser beam to selectively melt the powder according to the designed model [11–13]. Secondly, Ti6Al4V has a weak tribological property. Atar et al. [14] showed that the wear resistance using the Al_2O_3 grinding pair of the 316 L and CoCrMo alloy was almost 2 and 24 times of the Ti6Al4V. A post-treatment method that can improve the tribological property of Ti6Al4V is urgently needed.

Cryogenic treatment (CT) is a mature post-treatment process, which is often used to improve the tribological and mechanical properties of Ti6Al4V. Gu et al. [15] pointed out that a small coefficient of friction (COF) and a high Vickers hardness can be obtained by adjusting the CT temperature and the soaking time. Li et al. [16] found that the cryogenic treated (CTed) Ti6Al4V exhibited low COF and wear rate under both dry and wet wear conditions. Singla et al. [17] indicated that CT at −196 °C for 24 h could improve the tribological behavior of Ti6Al4V ELL. However, many studies above focus on the forged and casted Ti6Al4V. Bartolomeu et al. [18] pointed out that the tribological behavior of Ti6Al4V fabricated by SLM is significantly different from those fabricated by hot pressing and casting. During SLM, the microstructure of Ti6Al4V is composed of a plenty of unstable acicular martensite (α' phase) due to the high cooling rate. To the best of the authors' knowledge, few studies were carried out to investigate the effect of CT on the tribological behavior for Ti6Al4V fabricated using SLM. In consequence, this study aims to investigate the effect of CT on the tribological characteristics of Ti6Al4V fabricated by SLM. Scanning electron microscopy (SEM) and X-ray Diffraction (XRD) was used to observe the microstructure and phase composition. Vickers hardness and wear tests were carried out to characterize the hardness and tribological properties. COF, wear surface morphology and wear rates were analyzed to determine the wear mechanism. Based on these methods, the feasibility of CT applied to Ti6Al4V fabricated by SLM is discussed in detail.

2. Experimental details

2.1. Materials and preparation

The pre-alloyed Ti6Al4V powder produced by gas atomization is used as the preparation materials, which is nearly spherical, as shown in Fig. 1 (a). The particle size is in the range of 12–118 μm, with an average size of 39.55 μm (See in Fig. 1(b)). The specific chemical composition is listed in Table 1.

The sample was fabricated using the SLM machine of EOS M280 under an Argon gas atmosphere with a Yb fiber laser of 200 W, a scanning speed of 1200 mm/s, a spot size of 100 μm, a layer thickness of 30 μm, and a hatch spacing of 140 μm. The scanning strategy is "stripe" rotated by 67°. SLM schematic diagram is shown inFig. 2 (a). The sample with a dimension of $10 \times 10 \times 15$ mm^3 was built on a substrate, as shown in Fig. 2 (b). Then it was cut from substrate using wire Electrical Discharge Machining (wire-EDM) and was divided into three specimens. The first one was kept intact for comparison, numbered as UNCT. The second and third ones were CTed at −196 °C for 2 h and 72 h, respectively, numbered as CT02 and CT72 (See in Fig. 2 (c)).

SLX-80 cryogenic system (see Fig. 3 (a)) provided by the Technical Institute of Physics and Chemistry, Chinese Academy of Sciences (CAS) was used for CT. And the specific process parameter is showed in Fig. 3 (b). Among them, the cooling rate was 1 °C/min. The temperature can be controlled by adjusting the amount of liquid nitrogen diffused into the workbox and monitored by a temperature sensor. According to Refs [15,19], the soaking time range of CT is generally selected to be 2 h–72 h. Only the shortest and longest soaking time to be studied is to explore whether CT within a short soaking period can affect the tribological behavior of Ti6Al4V

Table 1 – The specific chemical composition of Ti6Al4V powder (wt%).

Element	Ti	Al	V	C	Fe	N	H
wt%	Balance	5.5–6.75	3.5–4.5	≤0.10	≤0.30	≤0.05	≤0.015

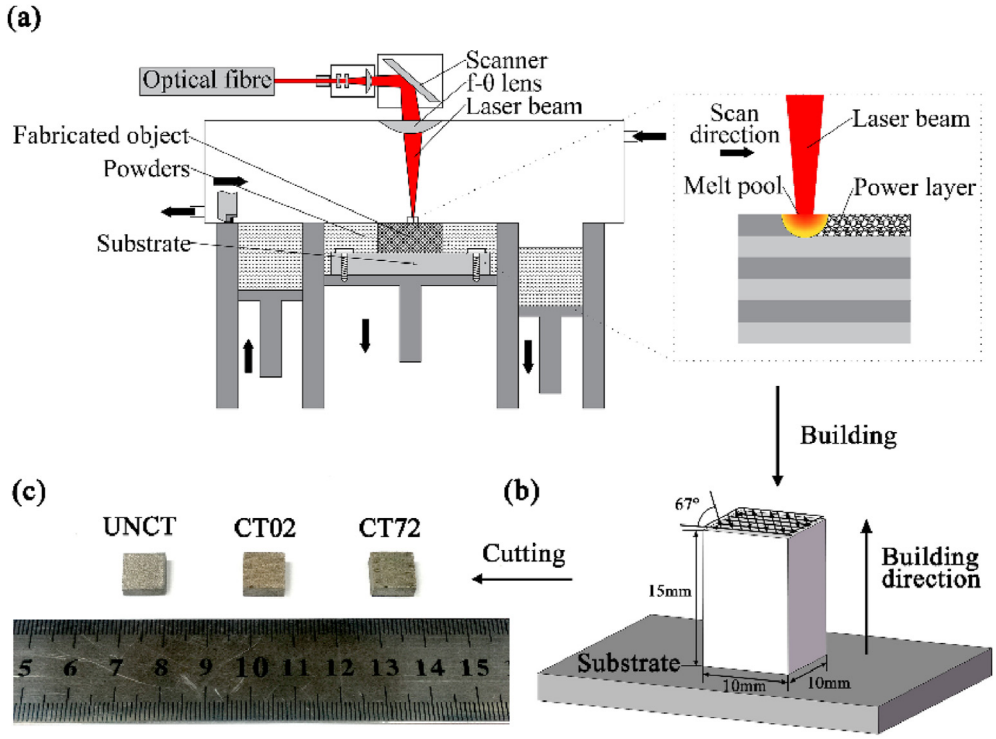

Fig. 2 – SLM process: (a) schematic diagram, (b) the sample built on the substrate and (c) divided into three specimens.

fabricated by SLM, and what is the reasons. After CT, the specimens were warmed to room temperature in the air.

2.2. Microstructure observation

Microstructure evolution and phase composition were performed using SEM (ZEISS GeminiSEM 500) and XRD (Bruker D8 Advance). The UNCT, CT02, and CT72 were ground with SiC papers down to 2000 mesh size, mechanically polished with diamond paste (1 μm), and etched with Kroll's reagent (5 ml HNO_3, 5 ml HF and 90 ml distilled water).

2.3. Vickers hardness test

Vickers hardness was measured using 423D Vickers Hardness Tester with an error range of ±2%, a loading force of 200 gf, and a duration time of 10 s. The hardness was measured at five points on each specimen and the average hardness value was obtained as the final result.

2.4. Wear test

The wear test was conducted in Phosphate Buffered Saline (PBS) fluid at 37 °C using an MS-T3000 type ball-on-disc rotation tribometer with a load of 5 N, a rotation radius of 3 mm, a rotation speed of 200 rpm, and a total wear duration of 60 min Al_2O_3 was selected as the grinding balls due to its property closest to the natural human bone [20]. During wear test, the actual wear condition of artificial hip joint in human body was simulated by controlling the wear environment, pressure and grinding ball material. Before the wear test, the UNCT, CT02, and CT72 were ground with SiC papers down to 2000 mesh size to obtain fine and uniform surface roughness (Ra, around 0.02 μm). The schematic diagram is shown in Fig. 4. According

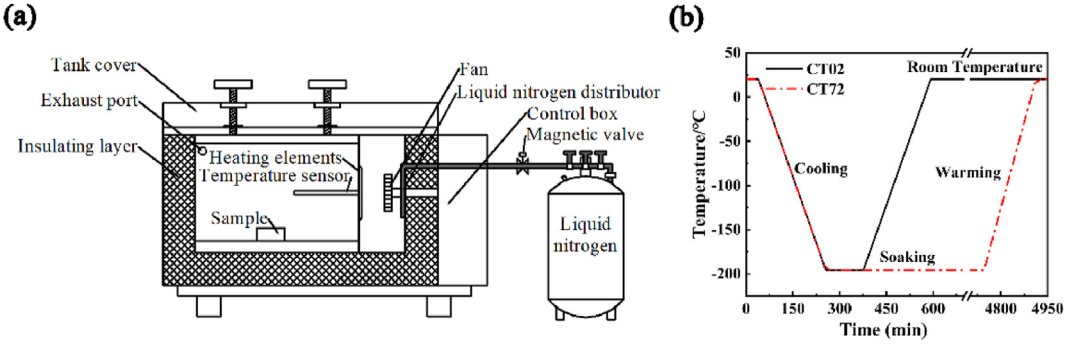

Fig. 3 – CT process: (a) schematic diagram and (b) process parameters.

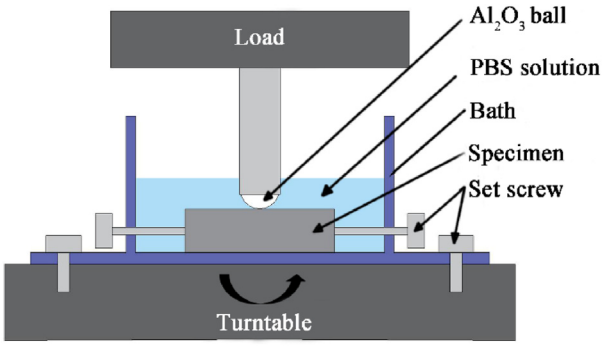

Fig. 4 – Schematic diagram of the wear test.

to the Hertzian theory calculation, the initial contact pressure is 0.93 GPa [21,22]. Furthermore, all the specimens were ultrasonically cleaned in alcohol for 20 min to remove the residual solution and wear debris before and after the wear test. SEM with X-Max^N Energy Dispersive X-Ray Spectroscopy (EDS) and ZYGO Nexview™ Scanning White-light Interferometry Profilometer were used to analyze the wear surface and element content. The wear test is carried out on the surface, which is perpendicular to the building direction. In order to avoid the experiment error caused by the uneven grains of different specimens, three repeated wear tests at least were carried out and the test results are recorded.

3. Results and discussion

3.1. Microstructure

Fig. 5 shows the microstructure evolution of the specimens for UNCT, CT02, and CT72. Many pores can be observed. The microstructure of UNCT mainly consists of α′ phase, as shown in Fig. 5 (a, b). Although, SLM process was carried out above the transition temperature of beta (β) phase (β_{tr} 995 ± 14 °C) [23] for all specimens. The β phase was transformed into α′ phase directly under a high cooling rate during SLM [24,25].

Being a super-saturated solid solution, α′ phase is metastable and tends to decompose into stable alpha (α) and β phases. The microstructure of CT02 is similar to the UNCT, which is mainly composed of α′ phase and a small amount of nanoscale white β phase distributed at the boundary of α′ phase, as shown in Fig. 5 (c, d). It can be deduced that the 2 h soaking time is not enough to provide the condition for α′ phase decomposition. As for the microstructure of CT72 (See Fig. 5 (e, f)), the α′ phase is decreased, and massive lath-like α phase appears with a nanoscale white β phase formed at the boundary of α′ phase. It can be known that α′ phase decomposition of α' → α + β occurs during CT for 72 h.

Fig. 6 shows the XRD result. No detectable peaks correspond to the β phase in UNCT. The peak position and strength of UNCT is consistent with Refs. [24–27]. The CT02 has a similar peak position and strength to UNCT. However, it has a slight fluctuation at the peak of (110) β and (220) β. This is consistent with the results of SEM. As for CT72, the α phase and α′ phase have similar lattice structure (close-packed hexagonal, HCP), so the peak corresponding to α does not change significantly. Ref. [28] presented a similar result. The peak corresponding to (100) α (002) α, and (101) α are increased, and the peaks corresponding to (110) β (211) β, and (220) β were detected. It can be concluded that α and β phases are formed when soaking time is extended to 72 h, and the CT72 experiences the decomposition of α′ phase [17].

Some researchers considered that the change of vanadium concentration in α′ phase is the cause of martensite decomposition [29,30]. The metallurgical difference between α and α′ phases is the amount of solute element in the atomic structure, which α′ phase is super-saturated in vanadium [31]. During CT, the low temperature reduces the solubility of vanadium in the α′ phase. Vanadium is a β phase stable element, which promotes the transformation of the metastable hexagonal close-packed structure (α′ phase structure) into a stable body-centered cubic structure (β phase structure). Therefore, β phase absorbs vanadium and nucleates along the boundary of the α′ phase [24,32]. Subsequently, the remaining α′ phase with insufficient vanadium is transformed into α phase gradually.

3.2. Vickers hardness

Vickers hardness of UNCT, CT02, and CT72 are 390.79 HV, 388.03 HV, and 371.34 HV, respectively, as shown in Fig. 7. The hardness of UNCT is higher than that in other studies (~320 HV) [16,33], resulting from a plenty of α′ phase existed in the specimens fabricated by SLM [16]. CT02 has a similar hardness value to UNCT, indicating that the short soaking time has little effect on the hardness of specimens. While, compared with UNCT, Vickers hardness of CT72 is reduced by 5.24%, which can be attributed to the microstructure evolution. The hardness of α′ phase is higher than that of α and β phases [31].

3.3. Wear test

Fig. 8 shows the result of COF. It can be seen that the COF of these specimens reaches a stable state after a quick climbing. While, a severe fluctuation exists in the stable state for the UNCT and CT02 (see Fig. 8 (a) and (b)). When the soaking time is increased to 72 h, the fluctuation is levelled off gradually, as shown in Fig. 8 (c). The average value of COF is 0.5497, 0.5201, and 0.4729, respectively (see in Fig. 8 (d)). The results of UNCT and CT02 are consistent with Ref. [18]. For the CT72, no evident fluctuation in the stable state and a small COF average value indicated that few abrasive particles and spalling pits exist on the wear surface [18,34].

Typical 3D profiler images of wear surface for these specimens are shown in Fig. 9. The UNCT has a severe wear damage with the maximum wear depth of 58.974 μm (see Fig. 9 (a)). The CT02 shows a similar wear damage to UNCT, with the maximum wear depth of 66.456 μm, as shown in Fig. 9 (b). However, for the CT72, the wear surface tends to flat and narrow, and the maximum depth of wear marks is 58.974 μm (see Fig. 9 (c)).

The wear rate of UNCT, CT02, and CT72 are 1.07×10^{-12} mm^3/Nm, 1.06×10^{-12} mm^3/Nm, and 0.82×10^{-12} mm^3/Nm, respectively, as shown in Fig. 10. The results show that the UNCT and CT02 have a similar volume loss, which are the

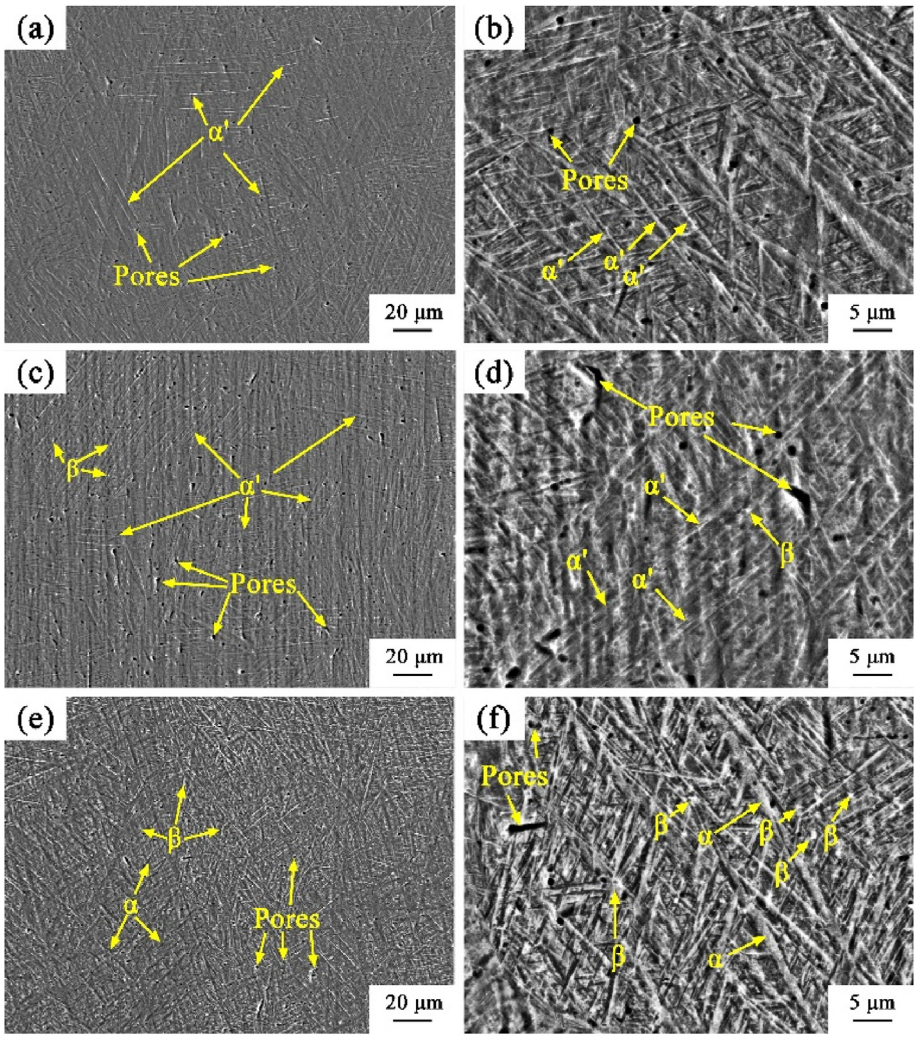

Fig. 5 – The microstructures of specimens (a, b) UNCT (c, d) CT02 (e, f) CT72.

most serious. It can be noted that the wear rate of CT72 decreases by 21.64% compared with UNCT.

To determine the wear mechanism of these specimens, the middle area morphologies of the wear surface were observed using SEM, as shown in Fig. 11. For the UNCT and CT02, the

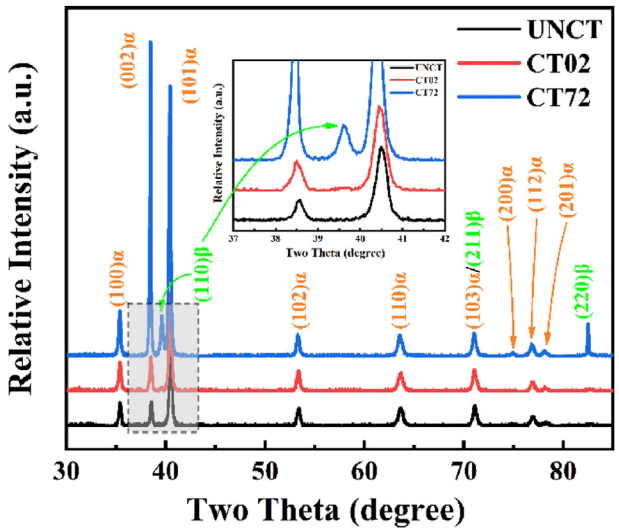

Fig. 6 – XRD diagram of specimens with and without CT.

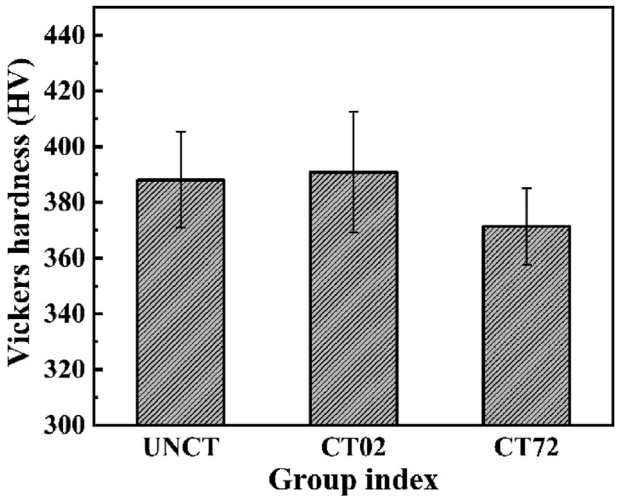

Fig. 7 – Results of Vickers hardness on specimens.

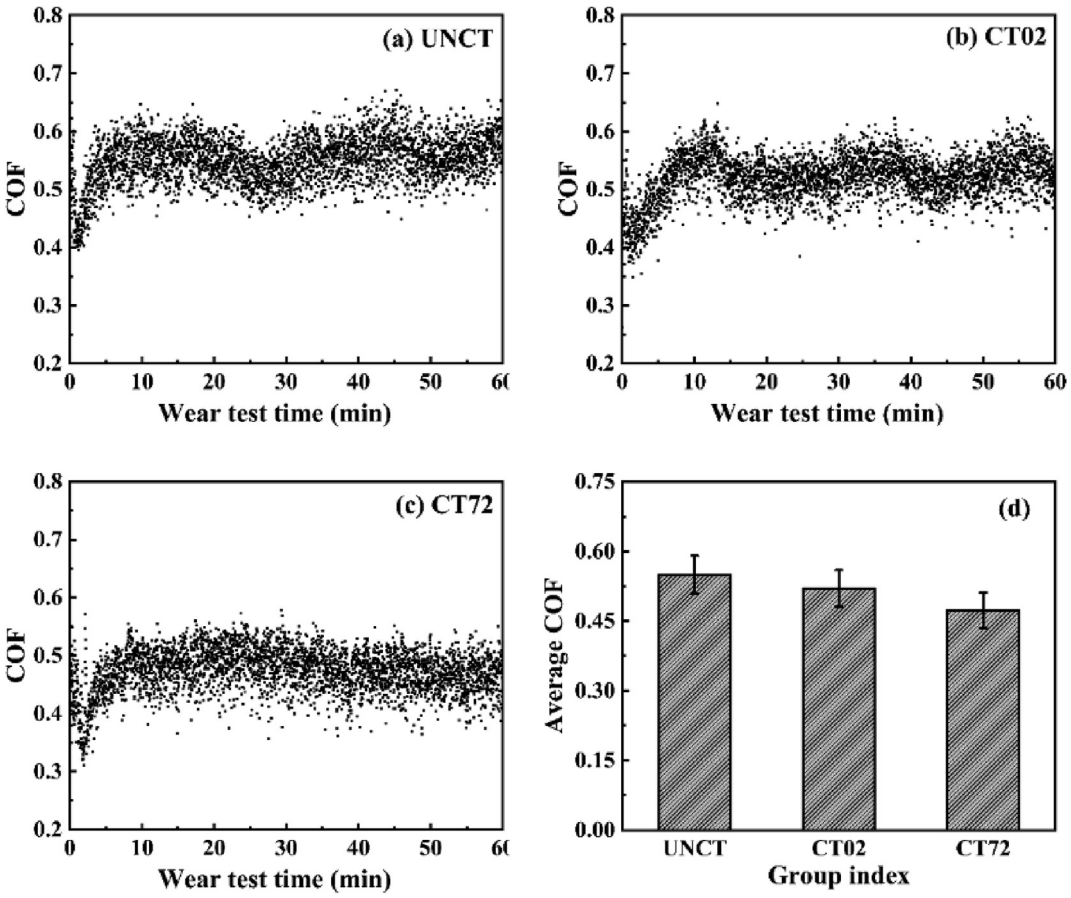

Fig. 8 – COF curve of (a) UNCT, (b) CT02, (c) CT72 and (d) average COF of the three specimens.

wear surface is composed of the deep and width ploughing grooves along the sliding direction as shown in Fig. 11 (a) and (c). The ploughing is caused by the coupling effect of abrasive particles. Except that, spalling, wear debris, the tongue-shaped wedges and microcracks can be observed in the enlarged views (see Fig. 11 (b) and (d)). The spalling and wear debris are caused by the UNCT adhered Al_2O_3 counter ball on under cyclic loading. Some wear debris may be adhered to Al_2O_3 counter ball and makes the ploughing severe. The presence of tongue-shaped wedges indicates that occurred during wear test. The severe plastic deformation and cycling load will cause stress concentration. Above all, the wear mechanism of UNCT and CT02 is the co-action of serious abrasive wear, adhesive wear, and fatigue wear. However, the wear surface of CT72 exhibits shallow ploughing grooves and a small amount of wear debris without evident the tongue-shaped wedges and microcracks (see Fig. 11 (e) and (f)) indicating a slight abrasive wear, as shown in.

The wear scar of Al_2O_3 counter ball was analyzed by SEM and EDS, as shown in Fig. 12. The counter balls of UNCT and CT72 are characterized by pits and island-like plateaus (see Fig. 12 (a) and (b)), where the pits are caused by wear. To analyze the island region, the distribution of titanium on the surface of the Al_2O_3 counter ball was observed, as shown in Fig. 12(c)–(d). The purple existed in each surface represents titanium and corresponds to the island-like plateaus. It can be

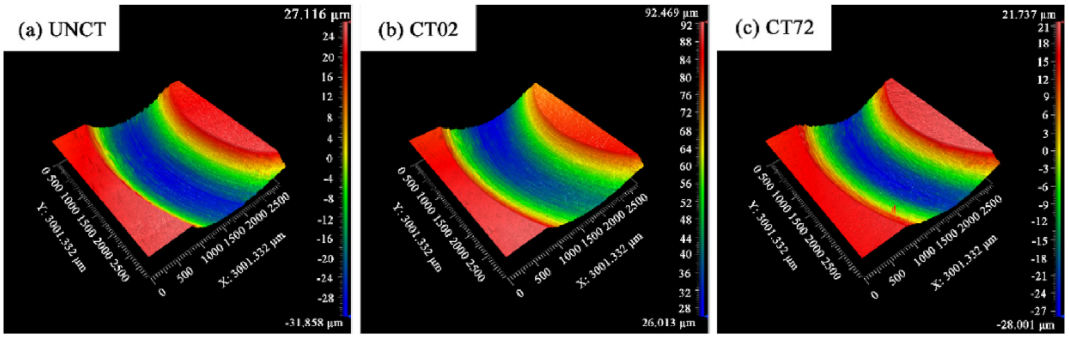

Fig. 9 – Typical 3D profiler images of wear surface: (a) UNCT, (b) CT02 and (c) CT72.

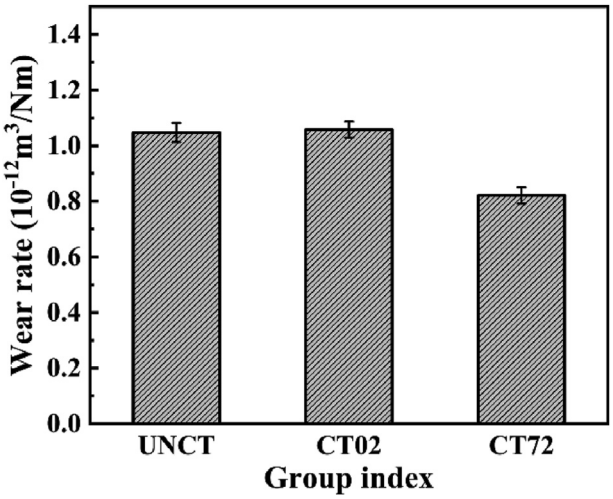

Fig. 10 – Wear rate of the three specimens.

inferred that wear debris of Ti6Al4V adheres to the surface of the Al_2O_3 counter ball causing the formation of island-like plateaus. Moreover, the titanium distributed on the surface of the CT72 counter ball Fig. 12 (d)) is less than that of UNCT (Fig. 12 (c)). Therefore, adhesive wear is no longer the dominant wear mechanism.

According to Archard's linear law [35], the tribological behavior is usually proportional to the hardness value of the specimen. In this study, although the hardness of CT72 is reduced, the tribological behavior is improved. It may because the α' phase decomposition dominates the improvement of tribological behavior, while, the hardness effect is weaker.

The decrease in wear rate is related to the change of wear mechanism caused by CT. For UNCT and CT02, the massive microcracks, spalling pits, and wear debris result in severe wear and make the wear rate increase. For CT72, the α' phase decomposition makes the wear mechanism transform to slight abrasive wear. It offers a fine wear condition to decrease the wear rate.

The COF is sensitive to the roughness of the contact surface between specimens and counter ball. A large amount of spalling pits and wear debris existed in the wear surface of UNCT and CT02 increase the contact surface roughness resulting in high COF with severe fluctuation (see Fig. 8 (a) and (b)). For CT72, the α' phase decomposition prevents the formation of microcracks and decreases the spalling pits as well

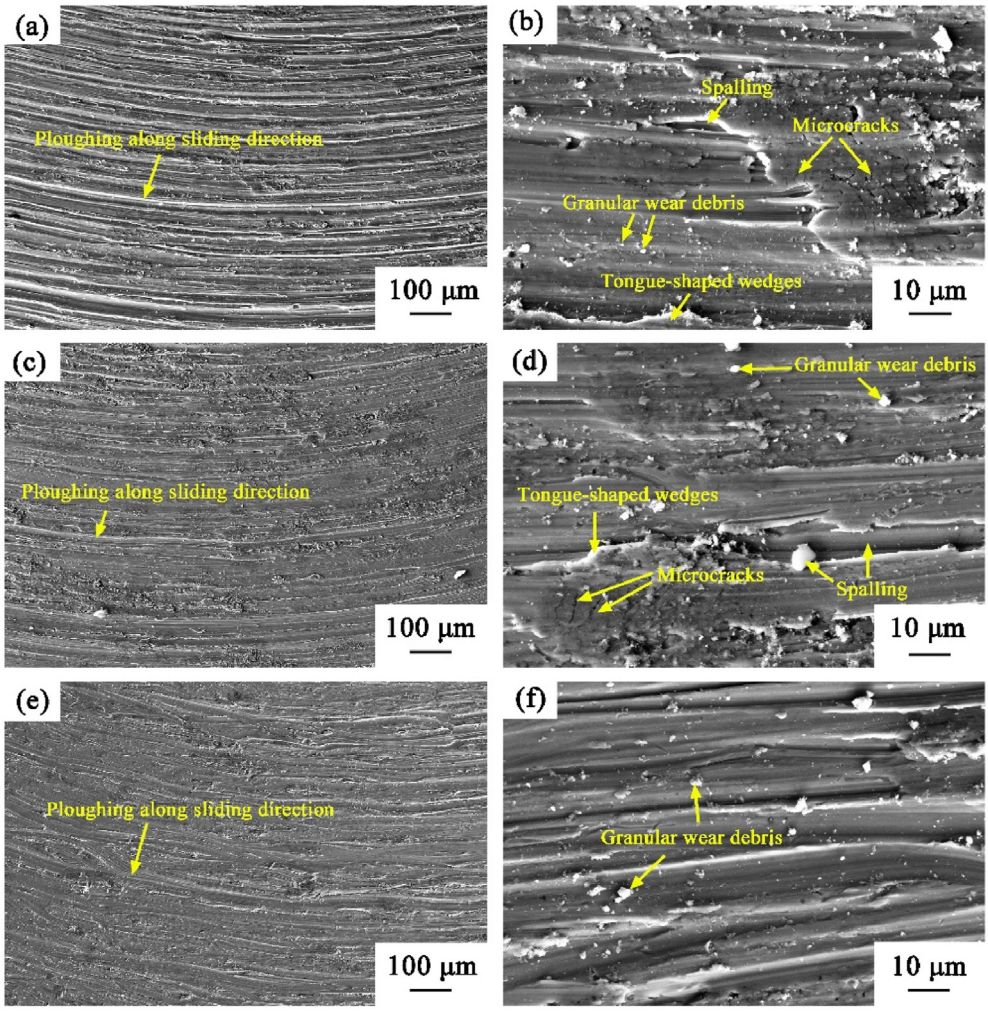

Fig. 11 – The microstructure of wear surface of specimens (a, b) UNCT (c, d) CT02 and (e, f) CT72.

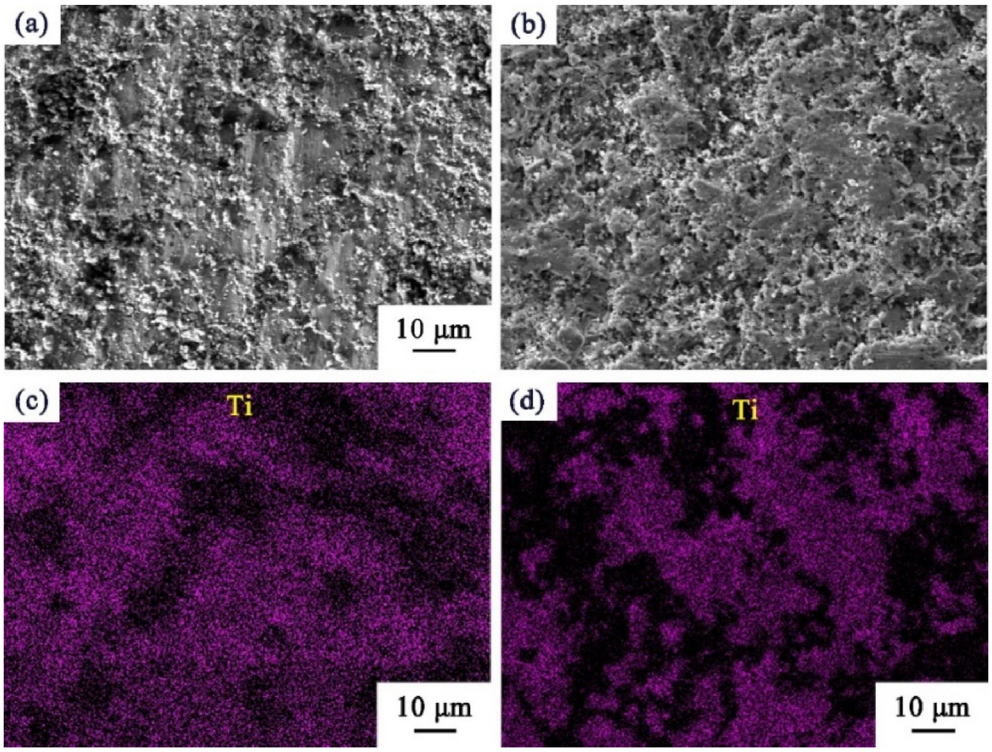

Fig. 12 – Microstructure and Ti distribution of wear scar of Al_2O_3 counter ball (a, c) UNCT and (b, d) CT72.

as wear debris. Therefore, CT72 has a relatively low average COF with smooth fluctuation (Fig. 8 (c)).

4. Conclusion

In this paper, the effect of CT on the tribological behavior of the Ti6Al4V fabricated by SLM were studied. The microstructure, phase analysis, Vickers hardness, and wear tests were conducted to characterize the tribological properties. The SEM results show that the microstructure of UNCT and CT02 is mainly α' phase. While the CT72 is composed of α and β phase. The XRD analysis confirms that CT for 72 h induces α' phase decomposition ($\alpha' \rightarrow \alpha + \beta$). Vickers hardness of the specimens as-fabricated, CT for 2 h and 72 h are 390.79 HV, 388.03 HV, and 371.34 HV, the average coefficient of friction are 0.5497, 0.5201, and 0.4729, as well as the wear rate of three specimens are 1.07×10^{-12} mm^3/Nm, 1.06×10^{-12} mm^3/Nm, and 0.82×10^{-12} mm^3/Nm, respectively. The UNCT and CT02 have a similar wear mechanism, which is the co-action of severe abrasive wear, adhesive wear, and fatigue wear, in contrast, the CT72 is slightly abrasive wear.

Declaration of Competing Interest

We declare that we have no financial and personal relationships with other people or organizations that can inappropriately influence our work, there is no professional or other personal interest of any nature or kind in any product, service or company that could be construed as influencing the position presented in the review of the manuscript entitled, "Effect of cryogenic treatment on tribological behavior of Ti6Al4V alloy fabricated by selective laser melting".

Acknowledgments

This work was sponsored by the Postdoctoral Research Foundation of China (2019M660739) the National Natural Science Foundation of China (41572362), and the Fundamental Research Funds for the Central Universities (35832020060).

REFERENCES

[1] Reddy MRS, Shivakumar MS, Phad P. Int Orthop 2018;4:252–8.
[2] Pang Y, Zheng X, Pei F, Chen Y, Guo K, Zhao F. Med Sci Monit 2019;25:3655–61.
[3] Guerado E, Caso E. Injury 2016;47:16–26.
[4] Courpied JP, Caton JH. Int Orthop 2011;35:149–50.
[5] Daigle ME, Weinstein AM, Katz JN, Losina E. Best Pract Res Clin Rheumatol 2012;26:649–58.
[6] Myers CA, Laz PJ, Shelburne KB, Judd DL, Winters JD, Stevens-Lapsley JE, et al. J Biomech 2019;93:18–27.
[7] Viceconti M, Muccini R, Bernakiewicz M, Baleani M, Cristofolini L. J Biomech 2000;33:1611–8.
[8] Buciumeanu M, Almeida S, Bartolomeu F, Costa MM, Alves N, Silva FS, et al. Tribol Int 2018;119:157–64.
[9] Dantas TA, Abreu CS, Costa MM, Miranda G, Silva FS, Dourado N, et al. Mater Sci Eng C 2017;77:1104–10.
[10] Su YC, Luo C, Zhang ZH, Hermawan H, Zhu DH, Huang JB, et al. J Mech Behav Biomed Mater 2018;77:90–105.
[11] Kahlin M, Ansell H, Moverare JJ. Int J Fatig 2017;103:353–62.

[12] Mercelis P, Kruth JP. Rapid prototyping J 2006;12:254–65.
[13] Calignano F, Manfredi D, Ambrosio EP, Biamino S, Lombardi M, Atzeni E, et al. Proc IEEE 2017;4:1–20.
[14] Atar E. Kovove Mater 2013;51:183–8.
[15] Gu KX, Wang JJ, Zhou Y. J Mech Behav Biomed Mater 2014;30:131–9.
[16] Li YG, Wang XF, Yang SQ, Hou LF, Wei YH, Zhang ZJ, et al. Materials 2019;12:2850.
[17] Singla AK, Singh J, Sharma VS. J Mater Eng Perform 2019;28:5931–45.
[18] Bartolomeu F, Buciumeanu M, Pinto E, Alves N, Silva FS, Carvalho O, et al. Trans Nonferrous Metals Soc China 2017;27:829–38.
[19] Gu KX, Li ZQ, Wang JJ, Zhou Y, Zhang H, Zhao B, et al. Mater Sci Forum 2013;747–748:899–903.
[20] Khanna R, Kokubo T, Matsushita T, Takadama H. Mater Sci Eng C Mater Biol Appl 2016;69:1229–39.
[21] Qin WB, Yue W, Wang CB. RSC Adv 2015;5:53484–96.
[22] Zhang SJ, Yue W, Kang JJ, Wang YY, Fu ZQ, Zhu LN, et al. Wear 2019;430:137–44.
[23] Xu W, Brandt M, Sun S, Elambasseril J, Liu Q, Latham K, et al. Acta Mater 2015;85:74–84.
[24] Neikter M, Huang A, Wu X. Int J Adv Manuf Technol 2019;104:1381–91.
[25] He BB, Wu WH, Zhang L, Lu L, Yang QY, Long QL, et al. Vacuum 2018;150:79–83.
[26] Weng ZJ, Gu KX, Cui C, Cai HK, Z Liu X, Wang JJ. Mater Char 2020;165:110385.
[27] Safdar A, Wei LY, Snis A, Lai Z. Mater Char 2012;65:8–15.
[28] Silva S, Kerber LO, Amaral L, Santos C. Surf Coat Tech 1999;116–119:342–6.
[29] Leva ES, Caram R, Jardini AL, Fogagnolo JB. J Mech Behav Biomed Mater 2016;54:149–58.
[30] Vrancken B, Thijs L, Kruth JP, Humbeeck JV. J Alloys Compd 2012;541:177–85.
[31] Cecchel S, Ferrario D, Cornacchia G, Gelfi M. Adv Eng Mater 2020;22:2000359.
[32] Zhang WW, Qin PT, Wang Z, Yang C, Kollo L, Grzesiak D, et al. Materials 2019;12:782.
[33] Li GR, Qin T, Fei AG, Wang HM, Zhao YT, Chen G, et al. J Alloys Compd 2019;802:50–69.
[34] Iordanoff I, Seve B, Berthier Y. ASME J Tribol 2002;124:530–8.
[35] Ahmed T, Rack HJ. Mater Sci EngA 1998;243:206–11.